



## One-pot preparation of magnetic Fe@Ag bimetallic catalyst for the catalytic reduction of 4-nitrophenol

Hongliang Xia<sup>a</sup>, Ziling Peng<sup>b</sup>, Wei Wang<sup>a,\*</sup>, Fatang Tan<sup>a</sup>, Xinyun Wang<sup>a</sup>, Xueliang Qiao<sup>a</sup>

<sup>a</sup>State Key Laboratory of Material Processing and Die & Mould Technology, Huazhong University of Science and Technology, Wuhan, 430074, Hubei, China, Tel./Fax +86-27-87541540, email: weiwang@hust.edu.cn (W. Wang)

<sup>b</sup>Material and Engineering Structure Department, Yangtze River Scientific Research Institute, Wuhan 430010, Hubei, China

Received 5 June 2018; Accepted 6 November 2018

### ABSTRACT

In this study, a magnetic Fe@Ag bimetallic catalyst was synthesized via a facile one-pot method in the presence of excessive sodium borohydride (NaBH<sub>4</sub>). The as-synthesized Fe@Ag bimetal was characterized by X-ray diffraction (XRD), scanning electron microscope (SEM), transmission electron microscope (TEM), X-ray photoelectron spectroscopy (XPS) and vibrating sample magnetometer (VSM). The influences of Fe/Ag molar ratio and gum arabic (GA) on the catalytic activity of Fe@Ag bimetal were investigated. It was found that the FeAg<sub>3</sub>-0.14 wt% bimetal with Fe/Ag molar ratio of 1:3 and GA concentration of 0.14 wt% exhibited the best activity for catalytic reduction of 4-NP, giving a pseudo-first-order rate constant of 48.8 min<sup>-1</sup> g<sup>-1</sup>. The saturation magnetization (*M<sub>s</sub>*) of FeAg<sub>3</sub>-0.14 wt% was 5.6 emu/g, which ensured the catalyst could be easily separated and recycled using a magnet. Moreover, the catalytic activity and phase composition of FeAg<sub>3</sub>-0.14 wt% showed no obvious changes after five continuous runs, indicating its high stability and reusability. Ag shell coated on the surface of Fe core played a main role in the catalytic reduction of 4-NP and also inhibited the oxidation of Fe core, which can be illustrated by electrochemical potentials and heterogeneous nucleation during the synthetic process. Furthermore, the Langmuir-Hinshelwood (L-H) model was applied to explain the catalytic mechanism of Fe@Ag bimetal.

**Keywords:** Fe@Ag bimetal; Magnetic catalyst; Catalytic reduction; 4-nitrophenol; One-pot preparation

### 1. Introduction

A great number of organic pollutants widely exist in wastewaters discharged from pesticides, dyes, textiles, pharmaceuticals, petroleum, and other industries [1,2], which has posed a potential threat to top predator species including human beings through bioaccumulating and magnifying in the food chain [3]. As a common organic pollutant, 4-nitrophenol (4-NP) has the properties of high toxicity, difficulty of natural degradation, high chemical and biological stability [4,5]. Thus, the effective removal of 4-NP from water has become an urgent issue. Currently, numerous measures such as adsorption [6,7], photocatalytic degradation [8–10] and catalytic reduction [2,11] are exten-

sively employed to deal with organic pollutants in aqueous systems. Among these methods, the catalytic reduction is considered as one of the most efficient and economical technique [12], due to its easy operation, low cost, high effectiveness and without generating secondary pollution. Moreover, 4-aminophenol (4-AP), the reduction product of 4-NP, is also an important organic intermediate for the manufacture of analgesic and antipyretic drugs [13]. Therefore, it is of great significance to develop a low-priced catalyst with high activity for effective catalytic reduction of 4-NP.

Nanoscale zero-valent iron (NZVI) is an effective reagent for the remediation of wastewater, owing to low cost, high surface activity, magnetic recovery property and environmental friendliness [14]. However, naked NZVI easily tends to aggregate and be oxidized in air and water, leading to a decrease in catalytic activity [15]. To improve the dispersity and stability of NZVI, various organic and

\*Corresponding author.

inorganic materials including chitosan [16], carboxymethyl cellulose (CMC) [17], gum arabic (GA) [18], and silica [19] have been applied as capping agents to stabilize NZVI. While these capping agents can occupy the surface active sites of NZVI, and prevent reactant molecules from approaching the catalyst surfaces, thus decreasing the catalytic activity of NZVI [20]. Compared with NZVI, silver nanoparticles (Ag NPs) have higher stability and better activity for catalytic reduction of 4-NP [21]. However, the difficulty of recovery and high cost of noble metal Ag greatly limit its large-scale application.

Recently, the binary system of NZVI and Ag NPs has been put forward to overcome the limitation of single metal [22], in which NZVI act as a magnetic recyclable carrier, and Ag NPs are responsible for mainly providing the catalytic activity. Gupta et al. [23] proposed that both iron ions and silver ions were reduced by ascorbic acid to form Fe-Ag bimetal, which caused some silver particles to be reversely capped by iron and decreased the catalytic activity for 4-NP reduction. Wang et al. [24] synthesized the Fe@Ag bimetallic particles by the replacement reaction between silver ions and NZVI. However, the low silver content in the prepared samples restricted the efficiency of removing organic pollutants, and the reusability of Fe@Ag bimetal was not discussed. According to the similar procedure, Lu et al. [25] obtained the Fe@Ag core-shell nanoparticles with Fe/Ag molar ratio of 52:48, but the catalytic properties have not been studied. In the replacement reaction between silver ions and NZVI, the preparation of Fe@Ag bimetal relies on NZVI as a reductant, usually giving a low silver content in product, which affects the achievement of high catalytic activity and stability [26,27].

In this work, Fe@Ag core-shell bimetallic catalyst was synthesized via a facile one-pot method using excessive sodium borohydride ( $\text{NaBH}_4$ ) as a reductant, in which large amounts of silver particles were deposited on the surface of Fe core. The catalytic performance of Fe@Ag bimetallic catalyst was evaluated by the reduction model of 4-NP with excessive  $\text{NaBH}_4$ . The influences of Fe/Ag molar ratio and GA on the catalytic activity of Fe@Ag bimetal were investigated. Also, the stability and reusability of Fe@Ag bimetallic catalyst were examined by successive recycling tests.

## 2. Experimental

### 2.1. Materials

Silver nitrate ( $\text{AgNO}_3$ ) was purchased from Henan Tongbai Xinhong Silver Products Co., Ltd. Iron (II) sulfate heptahydrate ( $\text{FeSO}_4 \cdot 7\text{H}_2\text{O}$ ) was obtained from Chengdu Kelong Chemical Reagent Co., Ltd. Gum arabic (GA), sodium borohydride ( $\text{NaBH}_4$ ) and 4-nitrophenol ( $4\text{-C}_6\text{H}_5\text{NO}_2$ ) were purchased from Sinopharm Chemical Reagent Co., Ltd. All chemicals were of analytical grade and used without further purification.

### 2.2. Catalyst preparation

Fe@Ag bimetallic catalyst was prepared by a facile one-pot method with excessive  $\text{NaBH}_4$  as a reductant. The whole reaction was conducted under mechanical stirring

and flushing argon. Firstly, 2.78 g  $\text{FeSO}_4 \cdot 7\text{H}_2\text{O}$  and a certain amount of GA were dissolved in 50 mL of oxygen-free water, and then transferred into a 250 mL three-necked flask. 50 mL of excessive  $\text{NaBH}_4$  solution was added dropwise into the mixture at room temperature. After the dropwise addition, the mixture was continuously stirred for 30 min to form Fe core. Next, the temperature of the mixture was controlled at 0–5°C with an ice-water bath. 50 mL of  $\text{AgNO}_3$  solution with different concentration, which make the corresponding theoretical molar ratio of Fe/Ag be 1:1, 1:2, and 1:3, was slowly dropped into the above mixture, and the reaction was continued for another 30 min. Finally, the resulting composites were separated from the reaction system using a permanent magnet and washed three times with oxygen-free water and ethanol, respectively. The as-prepared catalyst was dried in a vacuum oven at 40°C. The target products with different Fe/Ag molar ratios and GA dosage are denoted as  $\text{FeAg}_x\text{-y}$  wt%, where x is the theoretical molar ratio of Fe/Ag, and y is GA concentration in 150 mL reaction solution.

### 2.3. Characterization

X-ray diffraction (XRD) patterns of as-prepared samples were obtained using the Philips X'Pert PRO diffractometer. Morphology of samples was observed on a Gemini SEM300 scanning electron microscope (SEM) equipped with an X-ray energy dispersive spectrometer (EDS) at 20 kV. Microstructure of samples was explored using a TF20 transmission electron microscope (TEM). X-ray photoelectron spectroscopy (XPS) was performed on a Kratos/Axis Ultra DLD-600W spectrometer. Magnetic property of samples was analyzed by a JDAW-2000C&D vibrating sample magnetometer (VSM). UV-Vis spectrum was recorded using a Mapada UV-670 spectrophotometer.

### 2.4. Catalytic reduction of 4-NP

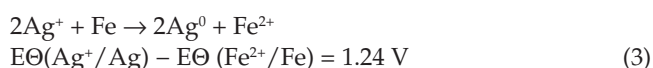
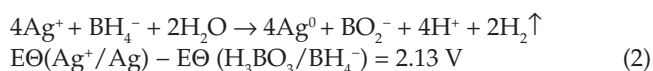
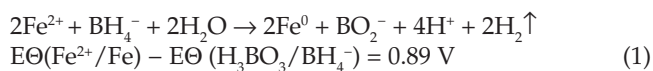
The catalytic performance of obtained Fe@Ag bimetallic catalyst was evaluated by the reduction of 4-NP using  $\text{NaBH}_4$  as a reductant at room temperature. Typically, fresh  $\text{NaBH}_4$  (5 mL, 0.2 M) was added to an aqueous solution of 4-NP (100 mL, 0.1 mM) under mechanical stirring. The solution color quickly changed from light yellow to bright yellow. Then 10 mg of Fe@Ag catalyst was added into the above solution. The yellow solution gradually faded as the catalytic reduction started. Meanwhile, about 3 mL of mixture was taken out and filtered by a 0.25  $\mu\text{m}$  membrane at suitable intervals, and the filtrate was measured by a UV-vis spectrophotometer in the wavelength range of 250–500 nm.

## 3. Result and discussion

### 3.1. Synthesis of Fe@Ag bimetallic catalyst

Regarding the synthesis of Fe@Ag bimetallic catalyst, the formation of Fe core and subsequent deposition of Ag shell on the surface of Fe core can proceed according to the following Eqs. (1), (2), and (3) [28]. These reactions are thermodynamically feasible processes relating to the standard electrode potentials ( $E^\ominus$ ) for  $\text{Ag}^+/\text{Ag} = 0.80$  V,  $\text{Fe}^{2+}/\text{Fe} = -0.44$  V, and

$\text{H}_3\text{BO}_3/\text{BH}_4^- = -1.33$  V vs. normal hydrogen electrode (NHE) [29,30]. Given that the standard potential difference of Eq. (2) is higher than that of Eq. (3), the added  $\text{AgNO}_3$  solution is preferentially reduced by surplus  $\text{NaBH}_4$  rather than  $\text{Fe}^0$  in theory.



During the reaction process, Ag is coated on the surface of Fe core by heterogeneous nucleation. Actually, silver ions near the surface of Fe core may be also reduced by  $\text{Fe}^0$  [Eq. (3)], and the generated ferrous ions will be immediately reduced by excessive  $\text{NaBH}_4$ . As a result, the facial iron on Fe core is partially re-dissolved and incorporated into silver shell until outside silver shell reaches a certain thickness.

Eventually, the coated silver effectively inhibits the continuous replacement reaction of inside iron core and silver ions to form Fe@Ag core-shell structure (Fig. 1).

### 3.2. Structure and morphology of Fe@Ag bimetallic catalyst

Fig. 2a shows the XRD patterns of as-prepared samples with different Fe/Ag molar ratio and GA concentration. Obviously, all diffraction peaks of these samples were well indexed to the face-centered cubic Ag (JCPDS 89-0597), indicating the samples did not contain impurities. The peaks at  $2\theta = 38.1^\circ, 44.3^\circ, 64.4^\circ, 77.4^\circ$  and  $81.5^\circ$  corresponded to the (111), (200), (220), (311) and (222) crystalline planes of Ag, respectively. The diffraction peaks related to metal oxide such as  $\text{Fe}_2\text{O}_3$ ,  $\text{Fe}_3\text{O}_4$  and  $\text{Ag}_2\text{O}$  were not detected, indicating that the metals in samples were not oxidized in the synthetic process. It should be noted that the characteristic peaks of Fe (JCPDS 85-1410) at  $2\theta = 44.4^\circ, 64.5^\circ$  and  $81.7^\circ$  were almost coincident with the (200), (220) and (222) crystalline planes of Ag. Furthermore, considering the X-ray shielding of silver shell [31], the characteristic peaks of Fe were weakened in the XRD patterns. Therefore, it is

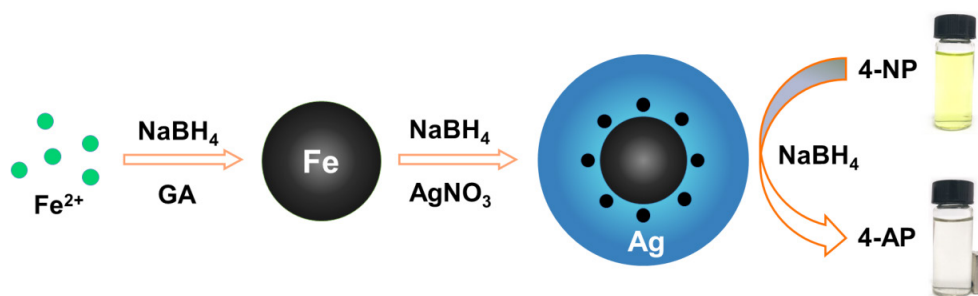


Fig. 1. Schematic illustration of one-pot approach to synthesize Fe@Ag bimetallic catalyst for 4-NP reduction.

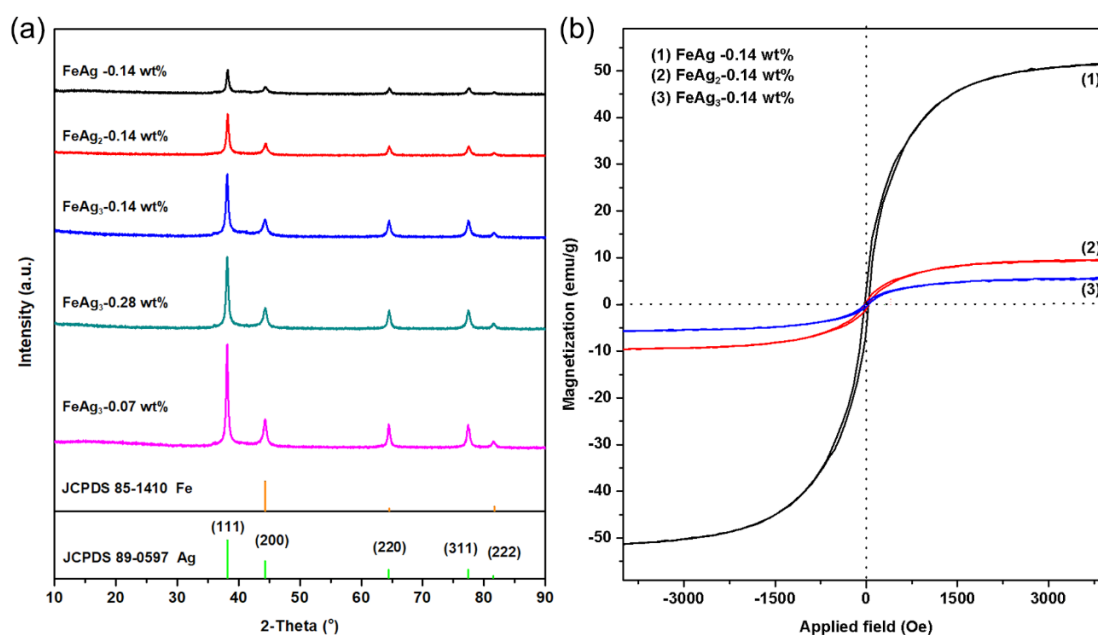


Fig. 2. XRD patterns (a) and magnetic hysteresis loops (b) of Fe@Ag bimetallic catalysts.

very difficult to identify the characteristic peaks of Fe in the XRD patterns. Notably, as the theoretical Fe/Ag molar ratio decreased, the intensity of characteristic peaks gradually became strong, demonstrating that an increasing content of Ag were successfully deposited on Fe core. Additionally, when the GA concentration decreased to 0.07 wt%, the XRD pattern of FeAg<sub>3</sub>-0.07 wt% possessed the strongest peaks as a result of the growth of the metallic particles [20]. While too much GA (0.28 wt%) maybe promote the formation of small metallic particles, that could aggregate together due to high surface energy [32], thus the characteristic peaks of FeAg<sub>3</sub>-0.28 wt% also became stronger compared to these of FeAg<sub>3</sub>-0.14 wt%.

As a common ferromagnetic metal, Fe component in the Fe@Ag bimetallic catalyst could be indirectly proved by the magnetic hysteresis loops (Fig. 2b). Due to the electromagnetic shielding effect of silver [25,33], the saturation magnetization of the catalyst became weaker with the decrease of theoretical Fe/Ag molar ratio, implying that the thickness of Ag shell increased. The saturation magnetization of FeAg-0.14 wt%, FeAg<sub>2</sub>-0.14 wt%, and FeAg<sub>3</sub>-0.14 wt% reached 51.5, 9.5, and 5.6 emu/g, respectively. Evidently, the magnetism of the sample with Fe/Ag molar ratio of 1:3 ensures the catalyst can be recovered by a magnet. When the molar ratio of Fe/Ag increased to 1:4, the as-prepared

sample was not responsive to a magnet, which indirectly confirmed more Ag was coated on the surface of Fe core.

The high-magnification SEM image of FeAg<sub>3</sub>-0.14 wt% (Fig. 3a) displays that the Ag particles on the iron surface were approximately spherical in shape, and these particles were about 70 nm in diameter. The EDS results in Fig. 3c and 3d reveal that silver was uniformly distributed on the sample surface, but the signal of iron was weak in view of the absorption of X-rays by silver particles coated on Fe surface [34].

TEM image (Fig. 4a) shows that the sizes of FeAg<sub>3</sub>-0.14 wt% nanoparticles were in the range of 55–75 nm, which was in accordance with the above SEM result. From HRTEM image (Fig. 4b), a silver layer with 4–6 nm thickness covered Fe core, suggesting the characteristic of core-shell structure for FeAg<sub>3</sub>-0.14 wt%. The inset picture shows a lattice spacing of 0.242 nm, which is assigned to (110) plane of Fe (JCPDS 85-1410). In a STEM HAADF mode, EDS mappings of FeAg<sub>3</sub>-0.14 wt% show the existence of Fe and Ag (Figs. 4c–e), similar to the SEM mappings.

### 3.3. Catalytic reduction of 4-NP by Fe@Ag bimetal with NaBH<sub>4</sub>

Catalytic reduction of 4-nitrophenol (4-NP) was chosen as a model reaction for evaluating the catalytic per-

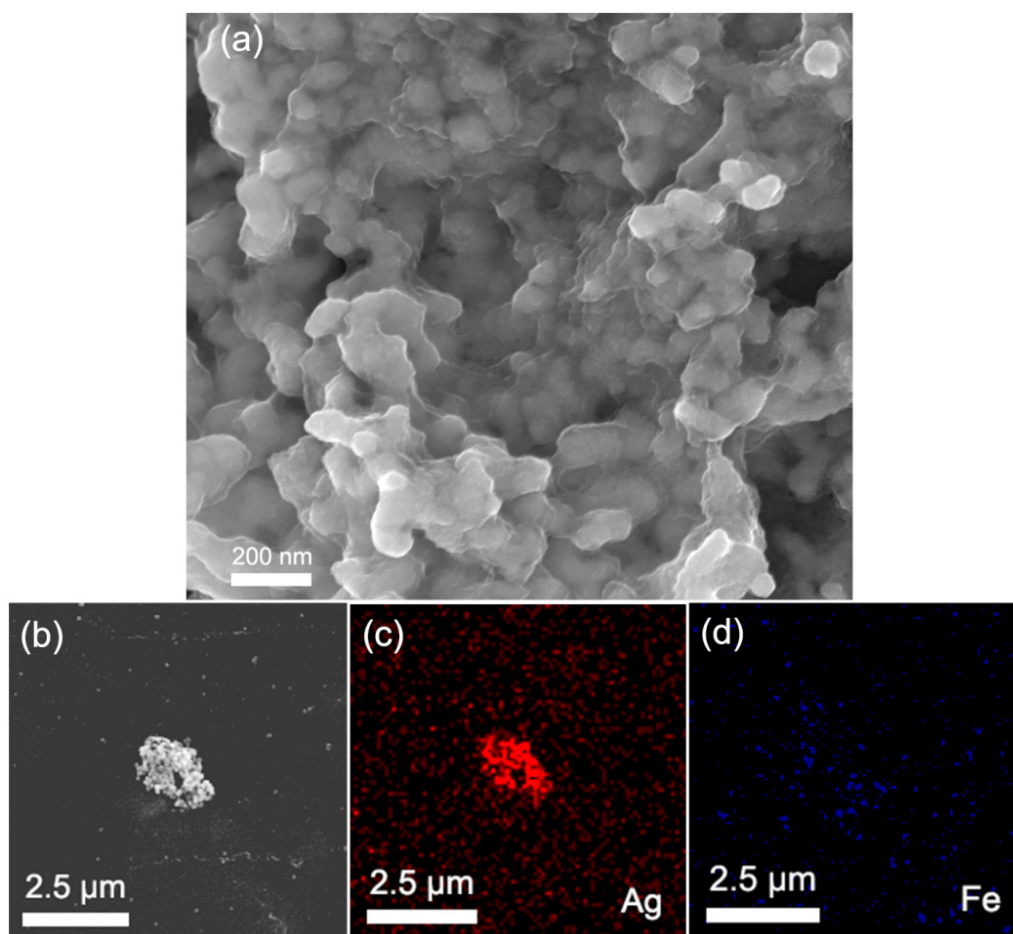


Fig. 3. SEM image and EDS elemental mappings of FeAg<sub>3</sub>-0.14 wt%.

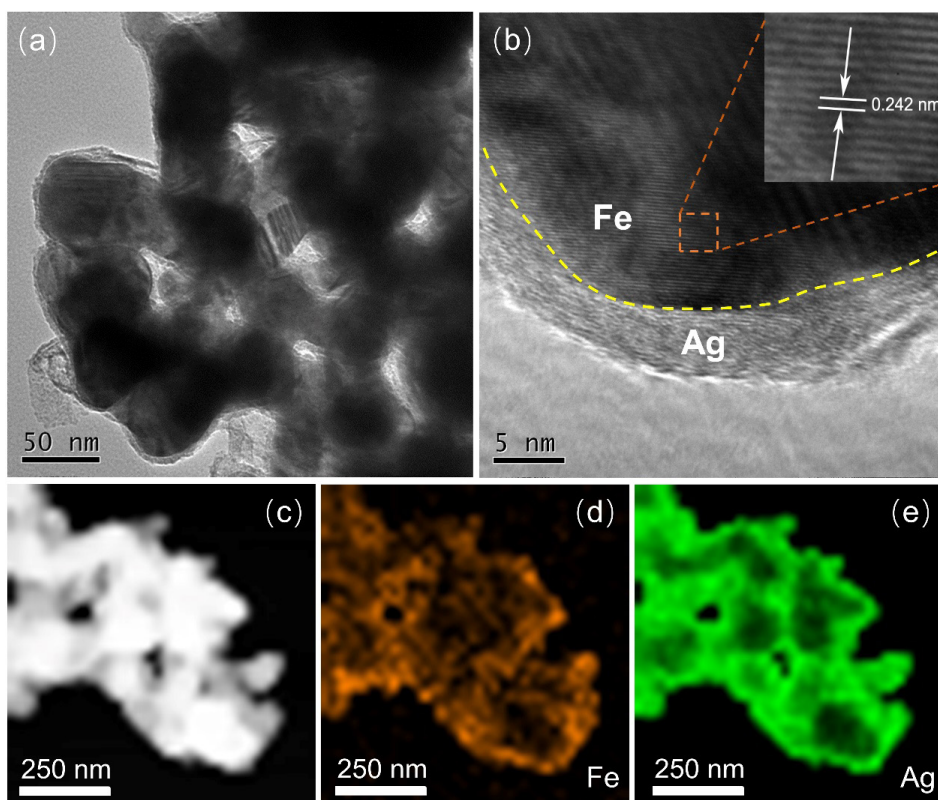


Fig. 4. TEM and HRTEM images (a, b), STEM HAADF image (c) and EDS mappings (d, e) of FeAg<sub>3</sub>-0.14 wt%.

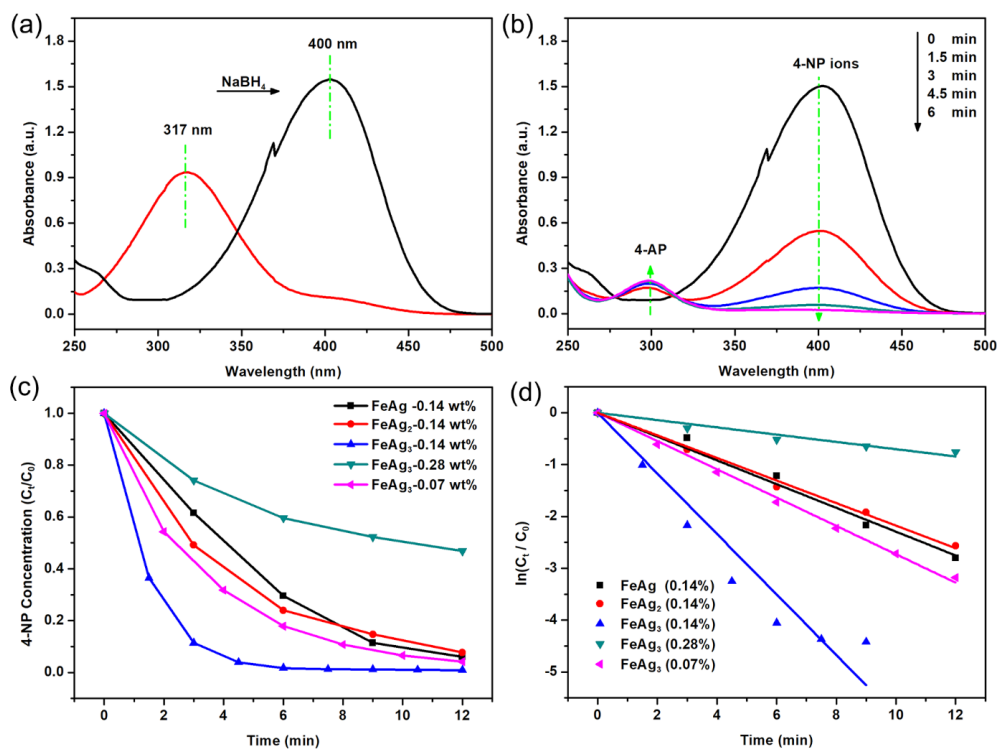


Fig. 5. (a) UV-vis spectra of 4-NP before and after adding NaBH<sub>4</sub> solution; (b) Successive UV-vis spectra for the reduction of 4-NP-catalyzed by FeAg<sub>3</sub>-0.14 wt% in the presence of NaBH<sub>4</sub>; (c) 4-NP relative concentration (C<sub>t</sub>/C<sub>0</sub>) and (d) the linear fitting of ln(C<sub>t</sub>/C<sub>0</sub>) vs. reaction time for catalytic reduction of 4-NP by Fe@Ag bimetal.

formance of as-prepared Fe@Ag bimetallic catalyst. As shown in Fig. 5a, 4-NP was converted to 4-NP ions after the addition of NaBH<sub>4</sub> solution, and the corresponding absorption peak shifted from 317 nm to 400 nm. Fig. 5b presents the time-dependent evolution of the UV-vis spectra for the reduction of 4-NP by NaBH<sub>4</sub> in the presence of FeAg<sub>3</sub>-0.14 wt%. The gradual weakness of the peak at 400 nm indicated that the concentration of 4-NP decreased, while a new peak at 300 nm corresponding to the formation of 4-AP increased. The batch reduction experiments were carried out to explore the effect of different Fe/Ag molar ratio and GA dosage on the catalytic performance of Fe@Ag bimetal. As could be observed from Fig. 5c, the catalytic activity of Fe@Ag bimetal followed the order: FeAg<sub>3</sub>-0.14wt% > FeAg<sub>3</sub>-0.07 wt% > FeAg<sub>2</sub>-0.14 wt% > FeAg<sub>3</sub>-0.14 wt% > FeAg<sub>3</sub>-0.28 wt%. Apparently, when the molar ratio of Fe/Ag was 1:3 and the GA dosage was 0.14 wt%, FeAg<sub>3</sub>-0.14wt% catalyst exhibited the highest activity. The result demonstrated that silver was a main active ingredient for the catalytic reduction of 4-NP by Fe@Ag bimetal. Furthermore, too much GA could capped the active sites on the catalyst surface, which caused a decreased catalytic activity [35]. A suitable amount of 0.14 wt% GA could both prevent particle agglomeration and promote the catalytic activity.

$$\ln(C_t/C_0) = -k_{app}t \quad (4)$$

In order to further study the catalytic performance of Fe@Ag bimetal, the pseudo-first-order kinetics was used to evaluate the reaction rate of 4-NP reduction. Because the excess of NaBH<sub>4</sub> ensured that its concentration remained essentially constant during the reaction period, the reaction rate could be considered to be only related to the concentration of 4-NP. According to the kinetics Eq. (4), where  $t$  is the reaction time,  $C_0$  is the initial 4-NP concentration, and  $C_t$  is the 4-NP concentration at time  $t$ , the apparent rate constant ( $k_{app}$ ) could be obtained from the slope of zero-crossing linear fitting. Fig. 5d shows the linear relationship between  $\ln(C_t/C_0)$  and the reaction time, which followed the first-order reaction law. The  $k_{app}$  of FeAg<sub>3</sub>-0.14wt% was calculated to be 0.488 min<sup>-1</sup> (48.8 min<sup>-1</sup> g<sup>-1</sup>), superior to these of other catalysts (Table 1).

#### 3.4. Stability and reusability of Fe@Ag bimetallic catalyst

Compared with homogeneous catalyst, heterogeneous catalyst has a distinct advantage for being easily separated and recycled [4,39,40]. To investigate the reusability of Fe@Ag bimetallic catalyst, five consecutive cycling tests were conducted using FeAg<sub>3</sub>-0.14 wt% catalyst. For each run, freshly prepared 4-NP (100 mL, 0.103 mM) and NaBH<sub>4</sub> (5

Table 1  
Model kinetics parameters of catalytic reduction of 4-NP by different catalysts

Catalyst	NaBH <sub>4</sub> (mmol/L)	Dosage (mg/mL)	Apparent rate constant $K_{app}$ (min <sup>-1</sup> )	Inherent rate constant $K$ (min <sup>-1</sup> g <sup>-1</sup> )	R <sup>2</sup>	References
FeAg <sub>3</sub> -0.14 wt%	10.3	0.1	0.229	22.9	0.993	This work
FeAg <sub>2</sub> -0.14 wt%	10.3	0.1	0.217	21.7	0.998	This work
FeAg <sub>3</sub> -0.14 wt%	10.3	0.1	0.488	48.8	0.950	This work
FeAg <sub>3</sub> -0.28 wt%	10.3	0.1	0.070	7.0	0.977	This work
FeAg <sub>3</sub> -0.07 wt%	10.3	0.1	0.273	27.3	0.999	This work
Ag/Fe <sub>3</sub> O <sub>4</sub>	10.1	0.04	0.185	–	0.986	[13]
Micron-SiO <sub>2</sub> @Ag	10	0.17	0.21	–	–	[36]
Fe <sub>3</sub> O <sub>4</sub> @PS/PDA-Ag	49.9	0.1	0.393	–	–	[37]
PS Beads@Ag	10	0.5	0.32	–	–	[38]

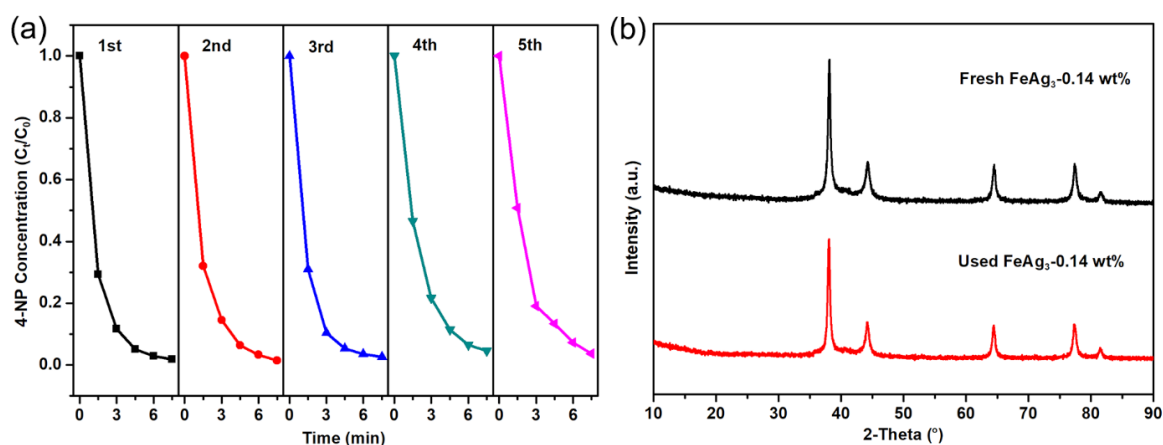


Fig. 6. (a) Recycling tests of FeAg<sub>3</sub>-0.14 wt%; (b) XRD patterns of FeAg<sub>3</sub>-0.14 wt% before and after use.

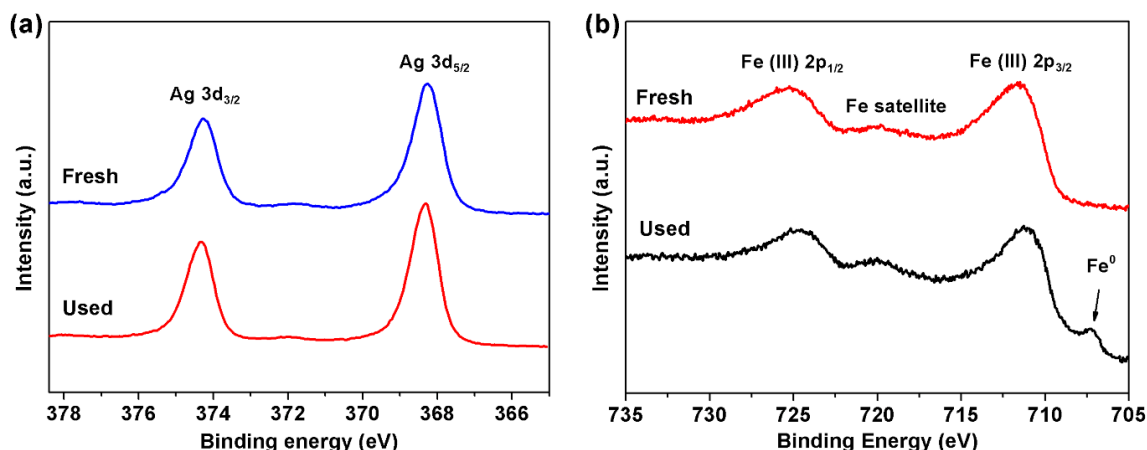


Fig. 7. Ag 3d (a) and Fe 2p (b) XPS spectra of the fresh and used FeAg<sub>3</sub>-0.14 wt%.

mL, 0.206 M) were added to the collected FeAg<sub>3</sub>-0.14 wt% catalyst. As shown in Fig. 6a, FeAg<sub>3</sub>-0.14 wt% catalyst still sustained high catalytic activity after five cycles, indicating its good reusability. To study the stability of a catalyst, the FeAg<sub>3</sub>-0.14 wt% samples before and after use were examined by XRD (Fig. 6b) for comparison. It could be seen that the diffraction peaks after 5 cycles stayed unchanged, which showed the high stability of FeAg<sub>3</sub>-0.14 wt%, owing to silver coating on the surface of iron core.

Further, the chemical composition and valence state of the fresh and used FeAg<sub>3</sub>-0.14 wt% was investigated by XPS technique. Compared to the fresh sample, there were no obvious changes in characteristic peaks of Ag 3d and Fe 2p, demonstrating that the catalyst remained unchanged after use, which ensured that the catalyst can be recycled for multiple times. In Ag 3dXPS spectra (Fig. 7a), the two peaks were located at 368.3 eV and 374.3 eV, corresponding to Ag 3d<sub>5/2</sub> and 3d<sub>3/2</sub> of Ag<sup>0</sup> [4]. In Fe 2p XPS spectra (Fig. 7b), three broad peaks at 711.6 eV, 720.0 eV and 725.0 eV were attributed to iron oxides [41]. Additionally, only a weak peak appeared at 707.2 eV in the used sample, which may be due to the reduction of iron oxides by excessive NaBH<sub>4</sub> on the surface of catalysts.

### 3.5. Mechanism for catalytic reduction of 4-nitrophenol

The reaction of 4-NP reduction by NaBH<sub>4</sub> is thermodynamically feasible, whereas without the assistance of a catalyst the reduction rate is so slow that the absorbance of 4-NP at 400 nm remains unchanged even for several days [38]. Ballauff et al. [42] concluded that the rate constant decreases as the 4-NP concentration increases from 0.03 mM to 0.1 mM in the existence of excessive NaBH<sub>4</sub>. The Langmuir-Hinshelwood (L-H) model of heterogeneous reaction, in which both reactants are adsorbed on the catalyst surface before the reaction occurs, can exactly elucidate the above dependence of the rate constant on the 4-NP concentration [43]. The mechanism of the reduction of 4-NP by the Fe@Ag bimetallic catalyst can be explained by the L-H model [44–46]. As shown in Fig. 8, NaBH<sub>4</sub> (electron donor) along with 4-NP (electron acceptor) are firstly adsorbed at active sites of the Fe@Ag surface. Then, abundant hydride

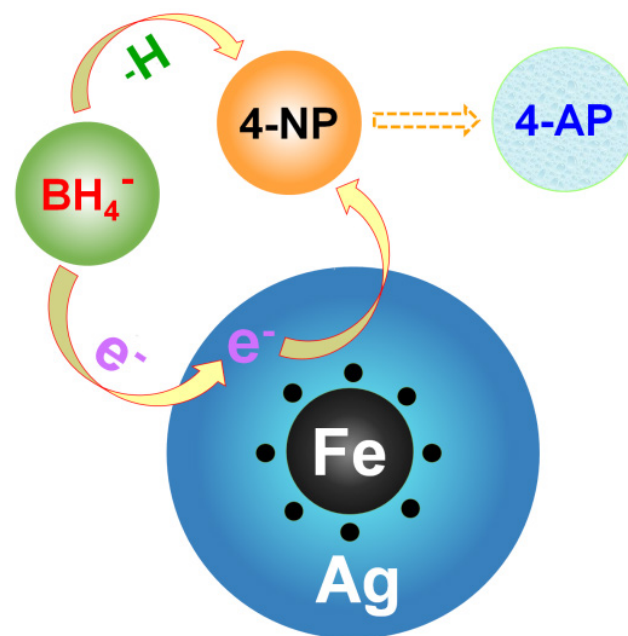


Fig. 8. Langmuir–Hinshelwood model for the reduction of 4-NP to 4-AP by NaBH<sub>4</sub> in the presence of Fe@Ag as a catalyst.

ions (H<sup>-</sup>) are released by the hydrolysis or decomposition of NaBH<sub>4</sub> with the aid of a catalyst. Finally, the generated hydride ions (H<sup>-</sup>) react with 4-NP to give 4-AP. Furthermore, the Fe@Ag catalyst as an electron relay can facilitate the transfer of electrons from NaBH<sub>4</sub> to 4-NP during the catalytic reaction.

## 4. Conclusions

In summary, the Fe@Ag bimetallic catalysts with different Fe/Ag molar ratios and GA dosage were facilely prepared by a one-pot method. The as-obtained Fe@Ag bimetal with good magnetic properties could be easily recovered by a magnet and showed excellent catalytic

activity for 4-NP reduction. Among these samples, the FeAg<sub>3</sub>-0.14 wt% bimetal exhibited the best catalytic activity for 4-NP reduction, and the pseudo-first-order rate constant reached 48.8 min<sup>-1</sup> g<sup>-1</sup>. The formation of Fe@Ag bimetal can be illustrated by electrochemical potentials and heterogeneous nucleation during the synthetic process. Ag shell coated on the surface of Fe core played a main role in the catalytic reduction of 4-NP and also inhibited the oxidation of Fe core. Furthermore, The Langmuir-Hinshelwood (L-H) model can well depict the catalytic mechanism of the Fe@Ag catalyst for 4-NP reduction. Easy preparation, high catalytic activity and good magnetic performance endow Fe@Ag bimetal to be a promising catalyst for removal of organic pollutants.

### Acknowledgements

The authors gratefully acknowledge the experimental help from Huazhong University of Science & Technology Analytical and Testing Center. X. Wang was supported by the National Science Foundation for Distinguished Young Scholars of China (No. 51725504).

### References

- [1] Z. Aksu, Application of biosorption for the removal of organic pollutants: a review, *Process. Biochem.*, 40 (2005) 997–1026.
- [2] W. Zhang, F. Tan, W. Wang, X. Qiu, X. Qiao, J. Chen, Facile, template-free synthesis of silver nanodendrites with high catalytic activity for the reduction of p-nitrophenol, *J. Hazard. Mater.*, 217–218 (2012) 36–42.
- [3] K.C. Jones, V.P. De, Persistent organic pollutants (POPs): state of the science, *Environ. Pollut.*, 100 (1999) 209–221.
- [4] X. Wang, F. Tan, W. Wang, X. Qiao, X. Qiu, J. Chen, Anchoring of silver nanoparticles on graphitic carbon nitride sheets for the synergistic catalytic reduction of 4-nitrophenol, *Chemosphere*, 172 (2017) 147–154.
- [5] G. Mele, R.D. Sole, G. Vasapollo, E. García-López, L. Palmisano, M. Schiavello, Photocatalytic degradation of 4-nitrophenol in aqueous suspension by using polycrystalline TiO<sub>2</sub> impregnated with functionalized Cu(II)-porphyrin or Cu(II)-phthalocyanine, *J. Catal.*, 217 (2003) 334–342.
- [6] S. Haydar, M.A. Ferro-García, J. Rivera-Utrilla, J.P. Joly, Adsorption of p-nitrophenol on an activated carbon with different oxidations, *Carbon*, 41 (2003) 387–395.
- [7] L. Ge, W. Wang, Z. Peng, F. Tan, X. Wang, J. Chen, X. Qiao, Facile fabrication of Fe@MgO magnetic nanocomposites for efficient removal of heavy metal ion and dye from water, *Powder Technol.*, 326 (2018) 393–401.
- [8] L. Ge, Z. Peng, W. Wang, F. Tan, X. Wang, B. Su, X. Qiao, P.K. Wong, g-C<sub>3</sub>N<sub>4</sub>/MgO nanosheets: light-independent, metal-poisoning-free catalysts for the activation of hydrogen peroxide to degrade organics, *J. Mater. Chem. A*, 6 (2018) 16421–16429.
- [9] D. Wu, W. Wang, F. Tan, F. Sun, H. Lu, X. Qiao, Fabrication of pit-structured ZnO nanorods and their enhanced photocatalytic performance, *RSC Adv.*, 3 (2013) 20054.
- [10] X. Song, W. Li, D. He, H. Wu, Z. Ke, C. Jiang, G. Wang, X. Xiao, The “midas touch” transformation of TiO<sub>2</sub> nanowire arrays during visible light photoelectrochemical performance by carbon/nitrogen coimplantation, *Adv. Energy Mater.*, 8 (2018) 1800165.
- [11] Z.G. Dai, X.H. Xiao, Y.P. Zhang, F. Ren, W. Wu, S.F. Zhang, J. Zhou, F. Mei, C.Z. Jiang, In situ Raman scattering study on a controllable plasmon-driven surface catalysis reaction on Ag nanoparticle arrays, *Nanotechnology*, 23 (2012) 335701.
- [12] H. Park, D.A. Reddy, Y. Kim, S. Lee, R. Ma, M. Lim, T.K. Kim, Hydrogenation of 4-nitrophenol to 4-aminophenol at room temperature: Boosting palladium nanocrystals efficiency by coupling with copper via liquid phase pulsed laser ablation, *Appl. Surf. Sci.*, 401 (2017) 314–322.
- [13] J.R. Chiou, B.H. Lai, K.C. Hsu, D.H. Chen, One-pot green synthesis of silver/iron oxide composite nanoparticles for 4-nitrophenol reduction, *J. Hazard. Mater.*, 248–249 (2013) 394–400.
- [14] S. Bae, S. Gim, H. Kim, K. Hanna, Effect of NaBH<sub>4</sub> on properties of nanoscale zero-valent iron and its catalytic activity for reduction of p-nitrophenol, *Appl. Catalysis B: Environ.*, 182 (2016) 541–549.
- [15] Z. Peng, C. Xiong, W. Wang, F. Tan, Y. Xu, X. Wang, X. Qiao, Facile modification of nanoscale zero-valent iron with high stability for Cr(VI) remediation, *Sci. Total Environ.*, 596–597 (2017) 266–273.
- [16] H. Lu, J. Chen, Z. Xiao, X. Qiao, F. Tan, W. Wang, Chitosan stabilised nanoscale zero-valent iron for the catalytic reduction of p-nitrophenol, *Micro Nano Lett.*, 9 (2014) 446–450.
- [17] Q. Wang, H. Qian, Y. Yang, Z. Zhang, C. Naman, X. Xu, Reduction of hexavalent chromium by carboxymethyl cellulose-stabilized zero-valent iron nanoparticles, *J. Contam. Hydrol.*, 114 (2010) 35–42.
- [18] T. Long, C.A. Ramsburg, Encapsulation of nZVI particles using a Gum Arabic stabilized oil-in-water emulsion, *J. Hazard. Mater.*, 189 (2011) 801–808.
- [19] P. Tartaj, C.J. Serna, Synthesis of monodisperse superparamagnetic Fe/Silica nanospherical composites, *J. Am. Chem. Soc.*, 125 (2003) 15754–15755.
- [20] Z. Niu, Y. Li, Removal and utilization of capping agents in nanocatalysis, *Chem. Mater.*, 26 (2014) 72–83.
- [21] S. Gu, W. Wang, F. Tan, J. Gu, X. Qiao, J. Chen, Facile route to hierarchical silver microstructures with high catalytic activity for the reduction of p-nitrophenol, *Mater. Res. Bull.*, 49 (2014) 138–143.
- [22] L. Ai, C. Zeng, Q. Wang, One-step solvothermal synthesis of Ag-Fe<sub>3</sub>O<sub>4</sub> composite as a magnetically recyclable catalyst for reduction of Rhodamine B, *Catal. Commun.*, 14 (2011) 68–73.
- [23] V.K. Gupta, M.L. Yola, T. Eren, F. Kartal, M.O. Çağlayan, N. Atar, Catalytic activity of Fe@Ag nanoparticle involved calcium alginate beads for the reduction of nitrophenols, *J. Mol. Liq.*, 190 (2014) 133–138.
- [24] Z. Wang, W. Huang, P.a. Peng, D.E. Fennell, Rapid dechlorination of 1,2,3,4-TCDD by Ag/Fe bimetallic particles, *Chem. Eng. J.*, 273 (2015) 465–471.
- [25] L. Lu, W. Zhang, D. Wang, X. Xu, J. Miao, Y. Jiang, Fe@Ag core-shell nanoparticles with both sensitive plasmonic properties and tunable magnetism, *Mater. Lett.*, 64 (2010) 1732–1734.
- [26] H. Wu, Q. Feng, H. Yang, E. Alam, B. Gao, D. Gu, Modified biochar supported Ag/Fe nanoparticles used for removal of cephalixin in solution: Characterization, kinetics and mechanisms, *Colloids Surf. A: Physicochem. Eng.*, 517 (2017) 63–71.
- [27] X. Nie, J. Liu, X. Zeng, D. Yue, Rapid degradation of hexachlorobenzene by micron Ag/Fe bimetal particles, *J. Environ. Sci.*, 25 (2013) 473–478.
- [28] J. Shen, Z. Li, Q. Yan, Y. Chen, Reactions of bivalent metal ions with borohydride in aqueous solution for the preparation of ultrafine amorphous alloy particles, *Cheminform*, 24 (1993) 8504–8511.
- [29] S.G. Bratsch, Standard electrode potentials and temperature coefficients in water at 298.15 K, *J. Phys. Chem. Ref. Data*, 18 (1989) 1–21.
- [30] G. Milazzo, Table of standard electrode potentials, *J. Electrochem. Soc.*, 125 (1978) 261C.
- [31] C.Q. Tran, C.T. Chantler, Z. Barnea, M.D.d. Jonge, B.B. Dhal, C.T.Y. Chung, D. Paterson, J. Wang, Measurement of the X-ray mass attenuation coefficient of silver using the x-ray-extended range technique, *J. Phys. B: At. Mol. Opt. Phys.*, 38 (2005) 89–107.
- [32] P. Venkatesan, N. Puvvada, R. Dash, B.N.P. Kumar, D. Sarkar, B. Azab, A. Pathak, S.C. Kundu, P.B. Fisher, M. Mandal, The potential of celecoxib-loaded hydroxyapatite-chitosan nano-

- composite for the treatment of colon cancer, *Biomaterials*, 32 (2011) 3794–3806.
- [33] W. Wang, W. Li, C. Gao, W. Tian, B. Sun, D. Yu, A novel preparation of silver-plated polyacrylonitrile fibers functionalized with antibacterial and electromagnetic shielding properties, *Appl. Surf. Sci.*, 342 (2015) 120–126.
- [34] W. Duane, H. Fricke, W. Stenström, The absorption of X-rays by chemical elements of high atomic numbers, *Proc. Natl. Acad. Sci. U.S.A.*, 6 (1920) 607.
- [35] H. Hu, J.H. Xin, H. Hu, X. Wang, D. Miao, Y. Liu, Synthesis and stabilization of metal nanocatalysts for reduction reactions – a review, *J. Mater. Chem. A*, 3 (2015) 11157–11182.
- [36] M. Wang, D. Tian, P. Tian, L. Yuan, Synthesis of micron-SiO<sub>2</sub>@ nano-Ag particles and their catalytic performance in 4-nitrophenol reduction, *Appl. Surf. Sci.*, 283 (2013) 389–395.
- [37] F. Peng, Q. Wang, R. Shi, Z. Wang, X. You, Y. Liu, F. Wang, J. Gao, C. Mao, Fabrication of sesame sticks-like silver nanoparticles/polystyrene hybrid nanotubes and their catalytic effects, *Sci. Rep.*, 6 (2016) 39502.
- [38] S. Jana, S. Ghosh, S. Nath, S. Pande, S. Praharaj, S. Panigrahi, S. Basu, T. Endo, T. Pal, Synthesis of silver nanoshell-coated cationic polystyrene beads: A solid phase catalyst for the reduction of 4-nitrophenol, *Appl. Catalysis A: General*, 313 (2006) 41–48.
- [39] Z. Dai, X. Xiao, W. Wu, Y. Zhang, L. Liao, S. Guo, J. Ying, C. Shan, M. Sun, C. Jiang, Plasmon-driven reaction controlled by the number of graphene layers and localized surface plasmon distribution during optical excitation, *Light Sci. Appl.*, 4 (2015) e342.
- [40] Y. Wu, X. Liu, D. Han, X. Song, L. Shi, Y. Song, S. Niu, Y. Xie, J. Cai, S. Wu, J. Kang, J. Zhou, Z. Chen, X. Zheng, X. Xiao, G. Wang, Electron density modulation of NiCo<sub>2</sub>S<sub>4</sub> nanowires by nitrogen incorporation for highly efficient hydrogen evolution catalysis, *Nat. Commun.*, 9 (2018) 1425.
- [41] H. Wu, Q. Feng, Fabrication of bimetallic Ag/Fe immobilized on modified biochar for removal of carbon tetrachloride, *J. Environ. Sci.*, 54 (2017) 346–357.
- [42] S. Gu, S. Wunder, Y. Lu, M. Ballauff, R. Fenger, K. Rademann, B. Jaquet, A. Zaccone, Kinetic analysis of the catalytic reduction of 4-nitrophenol by metallic nanoparticles, *J. Phys. Chem. C*, 118 (2014) 18618–18625.
- [43] P. Zhao, X. Feng, D. Huang, G. Yang, D. Astruc, Basic concepts and recent advances in nitrophenol reduction by gold- and other transition metal nanoparticles, *Coord. Chem. Rev.*, 287 (2015) 114–136.
- [44] N. Jadbabaei, R.J. Slobodjian, D. Shuai, H. Zhang, Catalytic reduction of 4-nitrophenol by palladium-resin composites, *Appl. Catal. A, Gen*, 543 (2017) 209–217.
- [45] N.C. Antonels, R. Meijboom, Preparation of well-defined dendrimer encapsulated ruthenium nanoparticles and their evaluation in the reduction of 4-nitrophenol according to the Langmuir–Hinshelwood approach, *Langmuir*, 29 (2013) 13433–13442.
- [46] T. Aditya, A. Pal, T. Pal, Nitroarene reduction: a trusted model reaction to test nanoparticle catalysts, *Chem. Commun.*, 51 (2015) 9410–9431.